

## The Effect of Undercut Anchor Diameter on the Rock Failure Cone Area in Pullout Tests

Józef Jonak<sup>1</sup>, Robert Karpiński<sup>1\*</sup>, Andrzej Wójcik<sup>1</sup>, Michał Siegmund<sup>2</sup>

<sup>1</sup> Department of Machine Design and Mechatronics, Faculty of Mechanical Engineering, Lublin University of Technology, Nadbystrzycka 36, 20-618 Lublin, Poland

<sup>2</sup> KOMAG Institute of Mining Technology, Pszczyńska 37, 44-100 Gliwice, Poland

\* Corresponding author's e-mail: r.karpinski@pollub.pl

### ABSTRACT

The numerical analysis was conducted using the FEM ABAQUS software to establish the impact of various undercut anchor diameters on the rock breakout cone formation. The central focus of the investigations was on the rock breakout prism, which tends to be approximated to a cone or a quadrilateral pyramid, including its characteristic parameter, the angle of failure cone  $\alpha$ . Assuming that the embedment depth and the undercut anchor head angle were constant for the considered range of anchor head diameters, it remains unclear, however, precisely how the anchor head diameter affects the value of the failure cone angle, and thus the surface area of the full breakout prism. This conclusion stands in confirmation of our former considerations regarding the impact of the anchor head angle on the size of the breakout surface. Furthermore, it is supported by the results obtained from the mechanical model simulation of the anchor-rock system, where the anchor head angle and the effective embedment depth were determined as significant factors affecting the assumed rock breakout failure. The underlying aspect of the reported investigation was to evaluate the effectiveness of the non-conventional rock breakout technology performed with an undercut anchor, whose primary factors were both the pullout force and the assumed volume of the rock cone.

**Keywords:** rock mechanics, fracture mechanics, rock destruction, concrete breakout failure, numerical modelling of fracture

### INTRODUCTION

In engineering, anchors are primarily employed in fastening systems for fixing steel structures in concrete [1–4]. Their load-carrying capacity assessment typically involves an approximation model, assuming that the concrete breakout product formed during the anchor pullout is idealized as a prismatic cone. The breakout strength calculations are based on an idealized breakout prism [5], which is a convenient approximation. The prism angle is approximately  $35^\circ$  and its parameters are relative to the effective embedment depth of an anchor  $h_{ef}$  (Fig. 1).

Currently, however, according to updated standards, it is assumed that the failure surface is represented by a quadrilateral pyramid with its

apex situated in the anchor head, and the base on the concrete surface is equal to  $3h_{ef}$ .

By employing the computational prowess of numerical modeling methods [6–9] (e.g., Finite Element Method (FEM) [10–14] or Boundary Element Method (BEM) [15–17] or machine learning [18–20]) in conjunction with experimental research [21–24] we have developed a detailed understanding of the actual behavior of engineering structures and their optimization. What has emerged from the extensive laboratory research [25,26], theoretical analyzes [27–29] and FEM simulations [30–32] conducted to date on the subject is that the pullout anchor strength, also referred to as its load-carrying capacity, is affected by a number of other factors, such as mechanical parameters of concrete (e.g., [33–36]), effective

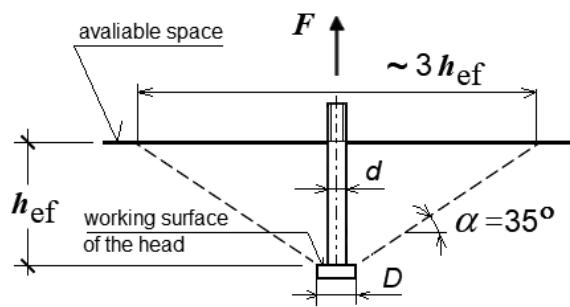


**Fig. 1.** Approximated concrete breakout cone for tension:  $h_{ef}$  – effective embedment depth,  $\alpha$  – breakout prism angle,  $d$  – anchor shaft diameter,  $D$  – anchor head diameter

embedment depth [37], the breakout anchor design [38,39], the anchor head geometry [40–44], or concrete reinforcement [45–50]. Numerous tests have been conducted in field and laboratory conditions that aimed to verify experimentally the results emerging from theoretical considerations [51,52]. These included analyzes devoted to the study of the group effect in anchorage systems on the value of the breakout force [53,54]. Concrete cracking mechanics has provided the basis for the development of mechanical models facilitating the interpretation of the anchorage effect on the material in which they are fastened [55,56]. Also, analytical models have significantly contributed to the understanding of the rock/concrete destruction mechanism induced by the pullout of mechanically [57,58] or chemically fastened anchors. These efforts have led to establishing new standards and recommendations for the estimation of the load capacity of anchors under specific application and load conditions [1].

In his work, Furche [59] has taken on to describe the volume of concrete surrounding the anchor separating from the member under tensile loading as a function of pressure generated on the working/bearing area of the anchor head. In particular, if the surface is sufficiently large, the local crushing of concrete does not occur in this area. Conversely, at the initial stage, a smaller head size leads to a reduction in the effective embedment depth as a result of assumed concrete crushing under the head, only at a later stage to result in the prism detachment from the concrete member. The tests were carried out at a changing width of the working area of the anchor head  $a$  (Fig. 2a,  $a = (D-d)/2$ ) from 0.5 mm to 4 mm. Based on these data, for  $h_{ef} = 80$  mm, the failure cone angle can be estimated at  $26^\circ$ . The change in pullout force

as a function of its displacement is shown in Figure 2b [59].

A range of experimental and numerical studies describe the influence of the embedment depth or the anchor head size on anchor performance (e.g., [39,54]). In general terms, the mean cone angle to the concrete surface  $\alpha$  has been determined to range between  $25^\circ$  and  $30^\circ$  [43]. According to [28], the angle of the concrete breakout prism  $\alpha$  is in the range of  $25^\circ$  to  $40^\circ$  to the concrete surface. Although on average, it amounts to approximately  $35^\circ$ , it has been shown, by e.g., [28,56], to increase when the embedment depth is deeper. What is more, it exhibits a slightly rising tendency at higher anchor head angles [43–45]. Nonetheless, it has been numerically and experimentally proven [60] that the average concrete breakout prism angle decreases with the increase in the anchor head size, whereas the diameter of the cone base (on the concrete surface) increases with the size of the head.

Conclusions similar to Furche [59] have been reported in a different study [61], which provided the evidence that, at pullout, smaller-headed anchors are prone to higher displacements at maximum loading than their larger head size counterparts. This trend is even stronger in greater embedment depth scenarios. As the size of the anchor head increases, the pullout load is observed to rise significantly while the displacement values show exactly the opposite tendency. The comparative analysis of the post-failure anchor performance displayed that at pullout with large-head-size anchors concrete becomes very brittle – it succumbs to sudden failure without prior noticeable displacement of the anchor. In the case of smaller heads, the concrete exhibits plastic properties, thus undergoing extensive deformations at the concrete-anchor interface.

Elsewhere [38], it has been shown that the application of bigger diameter anchor heads (from 35 mm to 52 mm) is reflected in the decrease in the mean compressive stress under the anchor head, which in turn resulted in a minor displacement of the anchor head. Hence, the smaller the head diameter, the greater the displacement at anchor pullout. It was also found that the breakout of the base material is mainly triggered by the failure of the concrete in tension (circumferential cracking) and not in compression. The onset of circumferential cracking progression is observed at roughly 30% of the failure load and shows high stability until reaching the failure load. At the post-failure

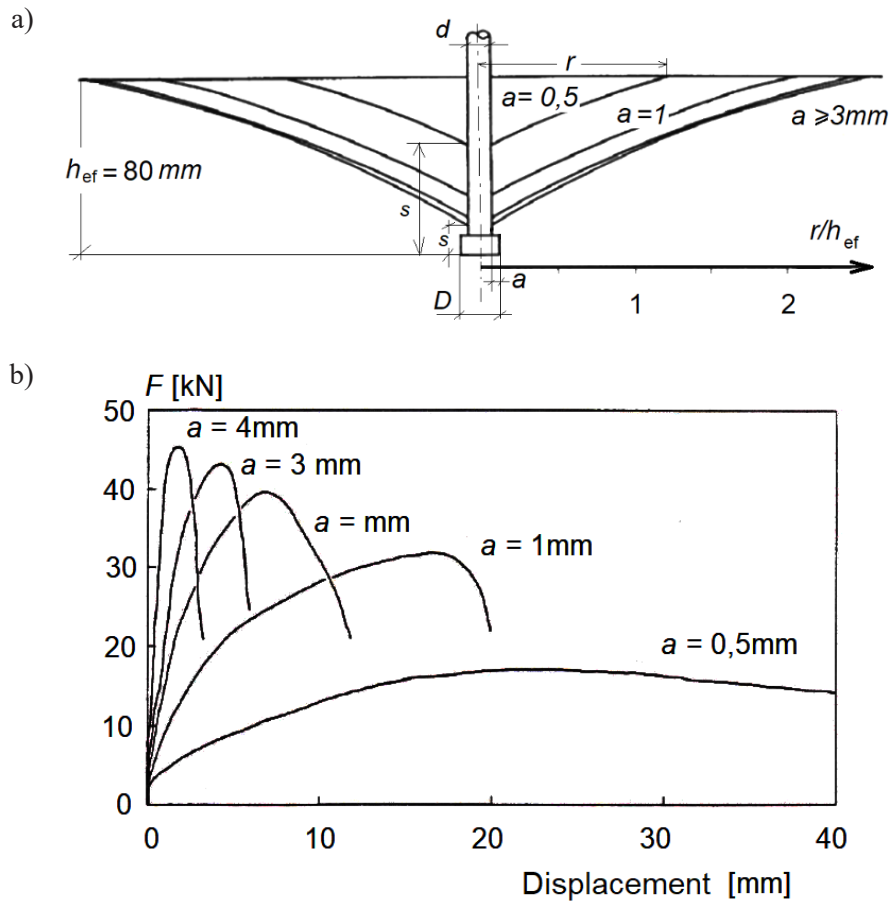


**Fig. 2.** The effect of anchor head width on the failure cone formation – a) and the change in the pullout force as a function of its displacement – b), based on Furche [59],  $s$  – the head displacement in the hole at failure load,  $r$  – radius of the failure cone base on the free surface of the rock,  $a$  – the width of the bearing area of the anchor head

stage, cracking becomes unstable, progresses rapidly, and forms a final breakout cone. The failure load is mainly dependent on the concrete fracture energy  $G_F$ , which is approximately the function of the square root of  $G_F$ . On the other hand, it appears (36) that the peak crack length is shorter for smaller anchor heads and the prism is of a more acute angle than in bigger-size anchor heads. Stress gradients in the vicinity of the anchor head are considered to be the main factors responsible for these differences. In addition, notable differences are observed in the main fracture, whose propagation closely resembles mode I (large heads) rather than the mixed mode (small heads). Non-reinforced concrete failure cone angles were shown [62] to range between  $20^\circ$  and  $25^\circ$  for embedment depths of 40-80 mm.

It is important to note that there is a clear dependence of the failure cone angle on the effective embedment depth. The anchor load-carrying capacity estimation model based on the variable cone angle  $\alpha$  assumption [63] introduces the following equation defining the failure cone angle as a function of the embedment depth:

$$\alpha = 28 + 0,134h_{ef} \text{ for } h_{ef} \leq 127 \text{ mm}$$

$$\alpha = 45^\circ \text{ for } h_{ef} > 127 \text{ mm}$$

Alternatively [56], the equation can take the following form:

$$\tan \alpha = 0.2h_{ef}^{0,25}$$

We propose the design of the undercut/breakout anchor for other-than-assembly applications, i.e., for the breakout of (solid) rock [64] where the anchor is initially fixed. In the tested breakout anchor, the bearing area of the undercut head is not perpendicular to the pullout load of the anchor, but is inclined at an angle  $\beta$  (see Figure 3).

Since the primary focus of the studies reported in the preceding paragraphs was on the effect of different diameters of the cylinder of headed studs (such as in [40] or Fig. 1), they do not fully explain the impact of the undercutting head diameter of the breakout anchor (Fig. 4) failure surface of the base material (including the failure cone angle  $\alpha$ ) where the anchorage is fixed. This factor may greatly alter the assumed breakout prism volume and, consequently, distort the

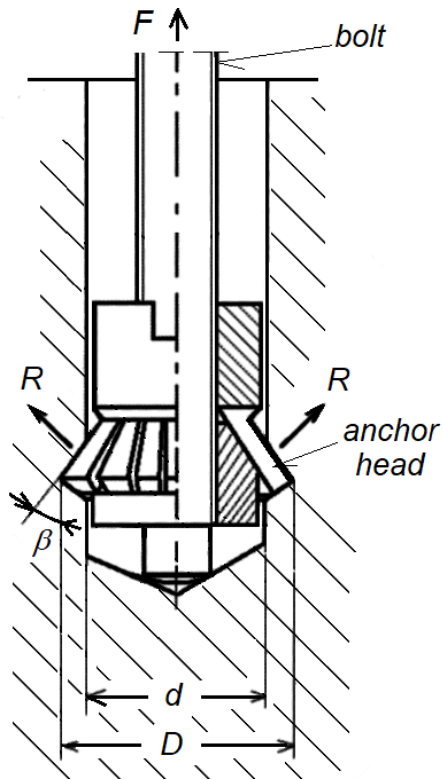


**Fig. 3.** The undercut/breakout anchor head:  $R$ , – anchor behavior in contact with the rock,  $\beta$  – angle of the cutting head,  $D$  – max. anchor diameter in the undercut,  $d$  – the diameter of the pre-drilled hole for the anchor,

calculations presenting the efficiency of the proposed method of detachment [37,64]. Hence, in order to address the knowledge gap, FEM numerical computations were involved. The results from these are presented in the following chapters of this study.

## MATERIALS AND METHODS

In an effort to explain how the application of undercut anchors of varying diameter affects the assumed surface of detachment (described by the failure cone angle  $\alpha$ ), it was initially established that only the following diameters would change:  $d$  (the diameter of the anchor hole) and  $D$  (the maximum undercut head diameter of the installed anchor), at a constant  $D/d$  ratio. It follows from the assumptions that the angle of the undercut head  $\beta$  is a constant value in all analyzed cases ( $\beta = \text{const.}$ ). The adopted dimensions  $d$  and  $D$  were characteristic for the considered undercut anchors (e.g., HDA-P Hilti anchor [4]) in the nominal range of dimensions M12, M16, and M20. Hence, the dimension  $d$  was equal to  $d = 22, 30, \text{ and } 37 \text{ mm}$  respectively. For the angle  $\beta = \text{const.} = 20^\circ$ , the dimension  $D$  is then  $D = 36.91, 44.91 \text{ and } 51.91$  respectively. Given the above assumptions, the mechanical model of the rock with the anchor hole adopted for simulations is shown in Figure 5. It is a flat axially-symmetric model, with the axis of symmetry along the anchor axis. The effective embedment depth was equal to  $h_{\text{ef}} = 50 \text{ mm}$ . The computations were performed using the FEM ABAQUS v.2022 software and its XFEM algorithm. Based on previous tests, the assumed surface of detachment on the free surface of the rock was approximately  $3h_{\text{ef}}$ . The dimensions of the base material model are the following:  $R = 500 \text{ mm}$  and  $H = 300 \text{ mm}$ .

The anchor head-rock contact area (the conical part of the undercut head (Fig. 6) was

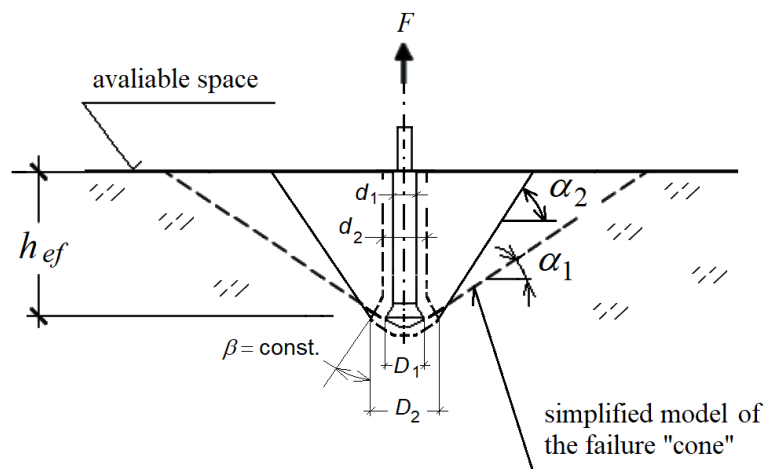


**Fig. 4.** Assumed influence of the undercut head diameter on the rock breakout anchor performance:  $D_1, D_2$  – maximum head diameter,  $d_1, d_2$  – diameter of the anchor hole,  $\alpha_1, \alpha_2$  – assumed failure cone angle,  $\beta$  – undercut head angle.

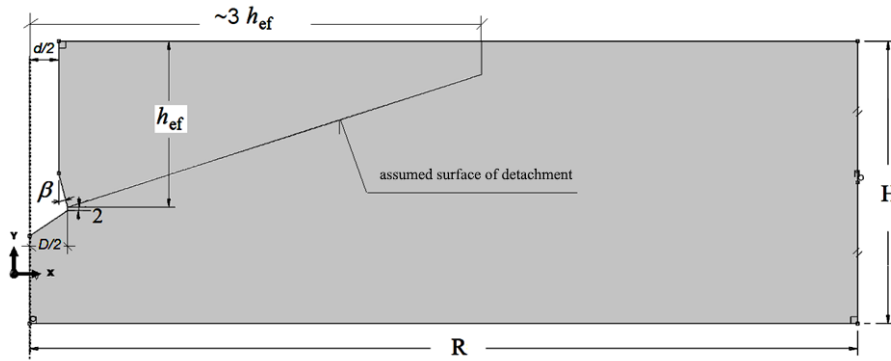


Fig. 5. Rock: a geometric model; H, R – model dimensions,  $h_{ef}$  – effective embedment depth,  $\beta$  – undercut head angle, d, D – considered characteristic head diameters

defined as the “Penalty contact,” derived from the ABAQUS library. The assumed coefficient of friction of steel against the rock (in the contact area) amounted to  $\mu = 0.2$ . The kinematic excitation of the anchor was applied along its Y axis. The anchor axis restraints, resulting from the model’s symmetric boundary conditions, were as follows: nodes on the right edge  $U1 = 0$  (deprived of all degrees of freedom in the OX axis), nodes in the model base  $U2 = 0$  (deprived of all degrees of freedom in the OY axis).

Material properties of the rock model: Young’s modulus – 14,275 MPa, Poisson’s number – 0.247, Failure mode – Max Principal Stress equal to  $f_t = 7.74$  MPa ( $f_t$  – tensile strength of the rock), Fracture Energy – 0.355. Stabilization factor 1E-06. Anchor model: Steel – material: Elastic, Isotropic, Elastic Modulus –  $E = 210,000$  MPa, Poisson’s Ratio –  $\nu = 0.3$ .

The finite element mesh of the model allowed for local densities. The global linear dimension of elements was 25 mm, in the contact area with the anchor – 2 mm, at the upper edges of the solid – the dimensions of the elements

vary from 3 to 10 mm, the line of the assumed fracture – 5 mm. The mesh was generated with the use of elements available in ABAQUS, such as Axisymmetric Stress, linear, Reduced integration, four-node mesh, and the element type CAX4R. The FE mesh for the rock base material itself is illustrated in Figure 7.

## RESULTS

Selected results from the numerical computations are shown in Figures 8÷9. Figure 8 demonstrates that the stress concentration  $\sigma_{max}$  is located in four areas of the model, i.e., the anchor head-rock contact area (compression), the area below the anchor in the model axis (tension), and the tensile stress in the area above the undercut and around the anchor hole can lead to propagation of radial cracks in the rock. What can be observed in the crack tip region is the typically strong concentration of tensile stresses that lead to fracture propagation at the crack tip.

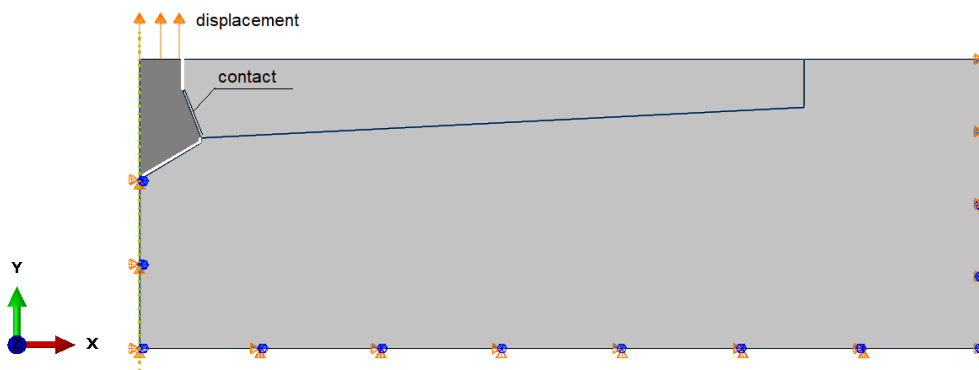
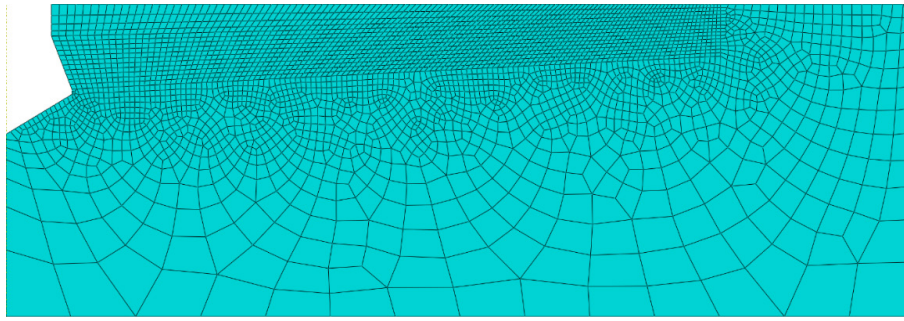
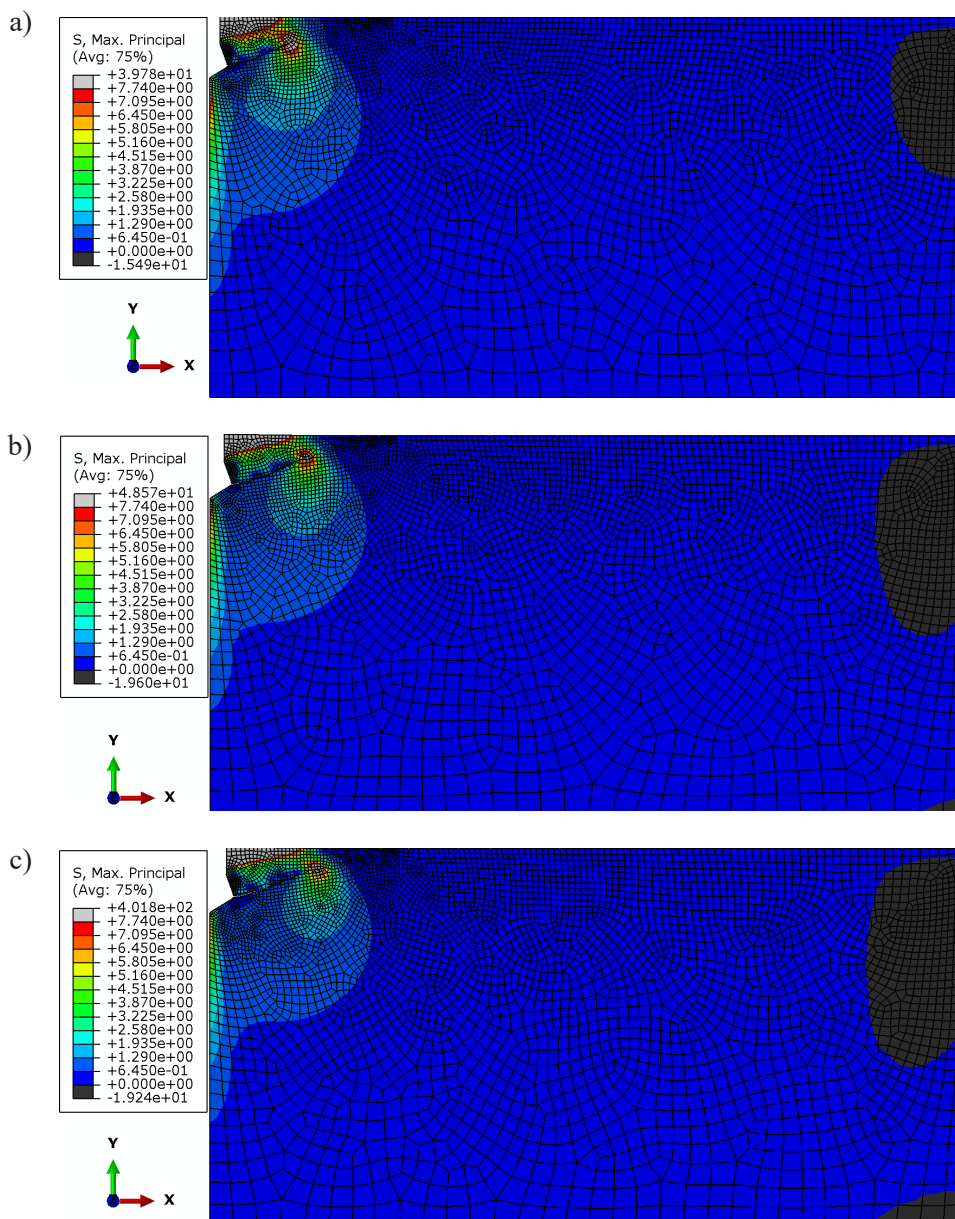


Fig. 6. Model boundary conditions, the location of the anchor head-rock contact area, and the kinematic excitation of the anchor head along the model’s OY axis



**Fig. 7.** The finite element mesh of the rock model with an undercut for the anchor head (the head model mesh turned off)



**Fig. 8.** Distribution of  $\sigma_{max}$  stress in the anchor head contact area. Anchor head diameter D equal to: a) 36.91, b) 44.91 c) 51.91mm (i.e., for M12, M16, and M20 anchors, respectively)

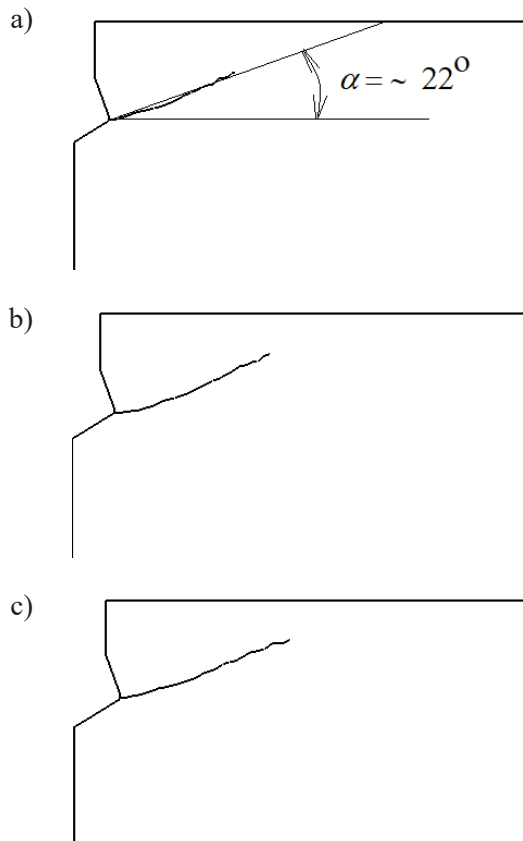


**Fig. 9.** The crack propagation trajectory under the pullout of an anchor head of a diameter  $D$ :  
 a) 36.91 mm, b) 44.91 mm, c) 51.91 mm  
 (i.e., for M12, M16, and M20 anchors respectively)

In the considered cases, the crack propagation angle  $\alpha$  at the initial phase amounted to approximately  $22^\circ$  relative to the free surface (or the plane perpendicular to the axis of the anchor), which is illustrated in Figure 9.

The failure mechanism that was recorded for the tested anchors in the numerical modeling tests above is confirmed by the one generated from the model of the anchor head impact on the rock base material presented below in Figure 10.

Due to the constants embedded in the model used in the simulation tests (i.e., the effective embedment depth  $h_{ef}$ , the undercut head angle  $\beta$ , the  $D/d$  ratio, the length of the undercut head cone element  $l$ ) and also given the fact that any alterations in the value of  $D$  and  $d$  were balanced by the adjustment of the anchor head size, the geometry of the undercut in the rock remained unchanged (and thus reflected the notch of constant geometric parameters). That is why, in the considered cases, neither the value of the angle  $\theta$  nor the anchor head bearing pressure on the rock  $P$  were affected. As a result, the crack propagated at an angle corresponding to the failure cone angle

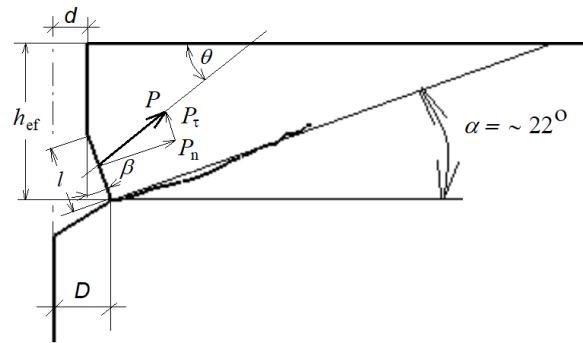


**Fig. 10.** A simplified model of the anchor head impact:  $P$  – anchor head bearing pressure on the rock (including friction),  $P_n$ ,  $P_t$  – normal and tangential components to the rock undercut surface,  $l$  – contact zone length ( $l = \text{const.}$ ),  $\beta = \text{const.}$  – undercut head angle,  $\theta$  – load direction in relation to the free surface of the rock base material,  $h_{ef} = \text{const.}$  – effective embedment depth

$\alpha$ . The described breakout mechanism is similar to the mechanism accompanying the cutting of rocks with mining tools [65].

## CONCLUSIONS

This paper reports on the results from the numerical calculations that set out to determine the influence of different undercut anchor diameters on the failure surface of rock in pullout tests. The following constants were established: the undercut head angle  $\beta$ , the effective embedment depth  $h_{ef}$ , the cone element length, the rock friction coefficient  $\mu$ , and the hole  $d$ , and the head diameter  $D$  ratio. Only the particular values of parameters  $d$  and  $D$  were changed by simulating the operation of the undercut anchors (e.g., HDA-P Hilti) in the nominal dimensions M12, M16, and M20.

The investigations revealed that the change in the undercut anchor diameter (in practice, corresponding to applying a larger size anchor from a given range of anchors) does not produce a significant change regarding the failure cone angle  $\alpha$  at the initial stage of crack propagation. Therefore, the assumed volume of detached rock is not likely to vary between the considered anchor diameter variants.

Given the sheer number of factors that could potentially contribute to the final breakout effect (including the combination of mechanical parameters of the rock or the rock breakout technological process parameters). These findings must be then interpreted with caution because further analyzes and experimental verification tests are required.

## Acknowledgements

This research project was financed in the framework of the Lublin University of Technology-Regional Excellence Initiative project, funded by the Polish Ministry of Science and Higher Education (contract no. 030/RID/2018/19).

## REFERENCES

1. Committee 355 ACI. Evaluating the Performance of Post-installed Mechanical Anchors in Concrete (ACI 355.2-01) and Commentary (ACI 355.2 R-01): An ACI Standard. In American Concrete Institute; 2002.
2. Eligehausen R. Connections between steel and concrete. Cachan: RILEM publications; 2001. (Proceedings).
3. Eligenhausen R, Hofacker I, Lettow S. Fastening technique current status and future trends International Symposium on Connections between Steel and Concrete. Stuttgart Sept. 2001;10.
4. HILTI. Technisches Handbuch der Befestigungstechnik für Hoch- und Ingenieurbau. Ausgabe; HILTI: Schaan, Liechtenstein, 2016.
5. Fuchs W, Eligehausen R, Breen JE. Concrete capacity design (CCD) approach for fastening to concrete. *Struct J*. 1995;92(1):73–94.
6. Valikhani A, Jaberi Jahromi A, Mantawy IM, Azizinamini A. Numerical Modelling of Concrete-to-UHPC Bond Strength. *Materials*. 2020 Mar 18;13(6):1379.
7. Sucharda O. Identification of Fracture Mechanic Properties of Concrete and Analysis of Shear Capacity of Reinforced Concrete Beams without Transverse Reinforcement. *Materials*. 2020 Jun 20;13(12):2788.
8. Cajka R, Marcalikova Z, Bilek V, Sucharda O. Numerical Modeling and Analysis of Concrete Slabs in Interaction with Subsoil. *Sustainability*. 2020 Nov 25;12(23):9868.
9. Sawa M, Szala M, Henzler W. Innovative device for tensile strength testing of welded joints: 3d modelling, fem simulation and experimental validation of test rig – a case study. *Appl Comput Sci*. 2021 Sep 30;17(3):92–105.
10. Falkowicz K. Composite plate analysis made in an unsymmetric configuration. *J Phys Conf Ser*. 2021 Dec 1;2130(1):012014.
11. Falkowicz K. Buckling numerical analysis of composite plate element in asymmetrical configuration. *J Phys Conf Ser*. 2021 Jan 1;1736(1):012029.
12. Falkowicz K. Effect of cut-out radius for behaviour of symmetrically laminated plates. *J Phys Conf Ser*. 2021 Jan 1;1736(1):012030.
13. Rogala M, Tuchowski W, Czarnecka-Komorowska D, Gawdzińska K. Analysis and assessment of aluminum and aluminum-ceramic foams structure. *Adv Sci Technol Res J* [Internet]. 2022;16(4). Available from: <http://www.astrj.com/Analysis-and-assessment-of-aluminum-and-aluminum-ceramic-foams-structure,153028,0,2.html>
14. Wyslowski P, Debski H, Falkowicz K. Stability analysis of laminate profiles under eccentric load. *Compos Struct*. 2020 Apr;238:111944.
15. Aliabadi MH. The boundary element method, volume 2: applications in solids and structures. Vol. 2. John Wiley & Sons; 2002.
16. Cheng AHD, Cheng DT. Heritage and early history of the boundary element method. *Eng Anal Bound Elem*. 2005;29(3):268–302.
17. Liu YJ, Mukherjee S, Nishimura N, Schanz M, Ye W, Sutradhar A, et al. Recent advances and emerging applications of the boundary element method. *Appl Mech Rev*. 2011;64(3).
18. Szabelski J, Karpiński R, Machrowska A. Application of an Artificial Neural Network in the Modelling of Heat Curing Effects on the Strength of Adhesive Joints at Elevated Temperature with Imprecise Adhesive Mix Ratios. *Materials*. 2022 Jan 18;15(3):721.
19. Rogala M, Gajewski J, Głuchowski D. Crushing analysis of energy absorbing materials using artificial neural networks. *J Phys Conf Ser*. 2021 Jan;1736:012026.
20. Gajewski J, Vališ D. Verification of the technical equipment degradation method using a hybrid reinforcement learning trees-artificial neural network system. *Tribol Int*. 2021 Jan;153:106618.
21. Bokor B, Sharma A, Hofmann J. Experimental investigations on concrete cone failure of rectangular and non-rectangular anchor groups. *Eng Struct*. 2019 Jun;188:202–17.
22. Hrubesova E, Mohyla M, Lahuta H, Bui T, Nguyen P. Experimental Analysis of Stresses in Subsoil below a Rectangular Fiber Concrete Slab †. *Sustainability*. 2018 Jun 28;10(7):2216.
23. Jendzelovsky N, Tvrda K. Probabilistic Analysis of a Hospital Building Slab Foundation. *Appl Sci*. 2020 Nov 6;10(21):7887.
24. Rogala M, Gajewski J, Gawdzińska K. Crashworthiness analysis of thin-walled aluminum columns filled with aluminum-silicon carbide composite foam. *Compos Struct*. 2022 Nov;299:116102.
25. Gontarz J, Podgórski J, Siegmund M. Comparison of crack propagation analyses in a pull-out test. In Lublin, Poland; 2018 [cited 2022 Jan 20]. p. 130011. Available from: <http://aip.scitation.org/doi/abs/10.1063/1.5019141>
26. Jonak J, Siegmund M. FEM 3D analysis of rock

- cone failure range during pull-out of undercut anchors. *IOP Conf Ser Mater Sci Eng*. 2019 Dec 19;710:012046.
27. Jonak J, Karpiński R, Siegmund M, Machrowska A, Prostański D. Experimental Verification of Standard Recommendations for Estimating the Load-carrying Capacity of Undercut Anchors in Rock Material. *Adv Sci Technol Res J* [Internet]. 2021 Jan 11; Available from: <http://www.astrj.com/Experimental-Verification-of-Standard-Recommendations-for-Estimating-the-Load-carrying,132279,0,2.html>
  28. Robson M, Lahouar A, Al-Mansouri O, Pinoteau N, Piccinin R, Abate M, et al. Simplified analytical fracture mechanics model for the evaluation of concrete cone capacity of a single headed stud and experimental validation on anchors with various embedment depths. In: *fib Symposium 2021: Concrete Structures: New Trends for Eco-Efficiency and Performance*. 2021.
  29. Morgan ASE, Niwa J, Tanabe T aki. Size Effect Analysis for Pullout Strength under Various Boundary Conditions. *J Eng Mech*. 1999 Feb;125(2):165–73.
  30. Jonak J, Karpiński R, Siegmund M, Wójcik A, Jonak K. Analysis of the Rock Failure Cone Size Relative to the Group Effect from a Triangular Anchorage System. *Materials*. 2020 Oct 19;13(20):4657.
  31. Jonak J, Siegmund M, Karpiński R, Wójcik A. Three-Dimensional Finite Element Analysis of the Undercut Anchor Group Effect in Rock Cone Failure. *Materials*. 2020 Mar 15;13(6):1332.
  32. Jonak J, Karpiński R, Wójcik A. Numerical analysis of undercut anchor effect on rock. *J Phys Conf Ser*. 2021 Dec 1;2130(1):012011.
  33. Ashour AF, Alqedra MA. Concrete breakout strength of single anchors in tension using neural networks. *Adv Eng Softw*. 2005 Feb;36(2):87–97.
  34. Jonak J, Karpiński R, Wójcik A, Siegmund M. The Influence of the Physical-Mechanical Parameters of Rock on the Extent of the Initial Failure Zone under the Action of an Undercut Anchor. *Materials*. 2021 Apr 8;14(8):1841.
  35. Jonak J, Karpiński R, Wójcik A, Siegmund M, Kalita M. Determining the Effect of Rock Strength Parameters on the Breakout Area Utilizing the New Design of the Undercut/Breakout Anchor. *Materials*. 2022 Jan 23;15(3):851.
  36. Karmokar T, Mohyeddin A, Lee J. Tensile behaviour of cast-in headed anchors in ambient-temperature cured geopolymer concrete. *Eng Struct*. 2022 Sep;266:114643.
  37. Jonak J, Karpiński R, Wójcik A. Numerical analysis of the effect of embedment depth on the geometry of the cone failure. *J Phys Conf Ser*. 2021 Dec 1;2130(1):012012.
  38. Ozbolt J, Eligehausen R. Numerical analysis of headed studs embedded in large plain concrete blocks. 1990;
  39. Ozbolt J, Eligehausen R, Reinhardt HW. Size effect on the concrete cone pull-out load. In: *Fracture Scaling*. Springer; 1999. p. 391–404.
  40. Bennett MS. Prediction of the shear cone geometry surrounding headed anchor studs. 1979;
  41. Jonak J, Karpiński R, Wójcik A. Influence of the Undercut Anchor Head Angle on the Propagation of the Failure Zone of the Rock Medium. *Materials*. 2021 May 2;14(9):2371.
  42. Jonak J, Karpiński R, Wójcik A. Influence of the Undercut Anchor Head Angle on the Propagation of the Failure Zone of the Rock Medium–Part II. *Materials*. 2021 Jul 12;14(14):3880.
  43. Nilforoush R, Nilsson M, Elfgren L. Experimental Evaluation of Influence of Member Thickness, Anchor-Head Size, and Orthogonal Surface Reinforcement on the Tensile Capacity of Headed Anchors in Uncracked Concrete. *J Struct Eng*. 2018 Apr;144(4):04018012.
  44. Nilforoush R, Nilsson M, Elfgren L, Ozbolt J, Hofmann J, Eligehausen R. Tensile capacity of anchor bolts in uncracked concrete: Influence of member thickness and anchor’s head size. *ACI Struct J*. 2017;114(6):1519–30.
  45. Nilforoush R, Nilsson M, Elfgren L. Experimental evaluation of tensile behaviour of single cast-in-place anchor bolts in plain and steel fibre-reinforced normal- and high-strength concrete. *Eng Struct*. 2017 Sep;147:195–206.
  46. A. Al- Ta S, A. Mohammed A. Tensile Strength of Short Headed Anchors Embedded in Steel Fibrous Concrete. *AL-Rafdain Eng J AREJ*. 2010 Oct 28;18(5):35–49.
  47. AlTaan SA, Mohammed AA, Al-Jaffal AA. Breakout Capacity of Headed Anchors in Steel Fibre Normal and High Strength Concrete. *Asian J Appl Sci*. 2012 Sep 15;5(7):485–96.
  48. Tóth M, Bokor B, Sharma A. Design recommendations for fasteners for use in steel fiber reinforced concrete. In: *Proceedings of the fib Symposium 2019: Concrete – Innovations in Materials, Design and Structures* [Internet]. 2019. p. 137–45. Available from: <https://www.scopus.com/inward/record.uri?eid=2-s2.0-85066069683&partnerID=40&md5=b25a97edaf478caeb86dae608e12c91f>
  49. Tóth M, Bokor B, Sharma A. Anchorage in steel fiber reinforced concrete – concept, experimental evidence and design recommendations for concrete cone and concrete edge breakout failure modes. *Eng Struct*. 2019 Feb;181:60–75.
  50. Bokor B, Tóth M, Sharma A. Fasteners in Steel Fiber Reinforced Concrete Subjected to Increased

- Loading Rates. *Fibers*. 2018 Dec 6;6(4):93.
51. Siegmund M, Jonak J. Analysis of the process of loosening the rocks with different strength properties using the undercutting bolts. *IOP Conf Ser Mater Sci Eng*. 2019 Dec 1;679(1):012014.
  52. Siegmund M, Kalita M, Bałaga D, Kaczmarczyk K, Jonak J. Testing the rocks loosening process by undercutting anchors. *Stud Geotech Mech*. 2020 Jul 9;42(3):276–90.
  53. Gontarz J, Podgórski J, Jonak J, Kalita M, Siegmund M. Comparison Between Numerical Analysis and Actual Results for a Pull-Out Test. [cited 2021 Mar 30]; Available from: <http://et.ippt.pan.pl/index.php/et/article/view/1005>
  54. Eligehausen R, Bouska P, Cervenka V, Pukl R. Size effect of the concrete cone failure load of anchor bolts. 1992;
  55. Yang KH, Ashour AF. Mechanism analysis for concrete breakout capacity of single anchors in tension. 2008;
  56. Zhao G. Tragverhalten von randfernen Kopfbolzenverankerungen bei Betonbruch. *Dtsch Aussch Fuer Stahlbeton*. 1995; (454).
  57. Piccinin R, Ballarini R, Cattaneo S. Linear Elastic Fracture Mechanics Pullout Analyses of Headed Anchors in Stressed Concrete. *J Eng Mech*. 2010 Jun;136(6): 761–8.
  58. Brincker R, Ulfkjær JP, Adamsen P, Langvad L, Toft R. Analytical model for hook anchor pull-out. In: *Proceedings of the International Symposium on Anchors in Theory and Practice: Salzburg, Austria, 9-10 October 1995*. CRC Press/Balkema; 1995. p. 3–15.
  59. Furche J. Zum Trag-und Verschiebungsverhalten von Kopfbolzen bei zentrischem Zug. *IWB*; 1994.
  60. Nilforoush R. A Refined Model for Predicting Concrete-Related Failure Load of Tension Loaded Cast-in-Place Headed Anchors in Uncracked Concrete. *Nord Concr Res*. 2019 Jun 1;60(1):105–29.
  61. Ožbolt J, Eligehausen R, Periškić G, Mayer U. 3D FE analysis of anchor bolts with large embedment depths. *Eng Fract Mech*. 2007 Jan;74(1–2):168–78.
  62. Gesoglu M, Özturan T, Özel M, Güneyisi E. Tensile behavior of post-installed anchors in plain and steel fiber-reinforced normal-and high-strength concretes. *ACI Struct J*. 2005;102(2):224.
  63. Farrow CB, Klingner RE. Tensile capacity of single anchors in concrete: Evaluation of existing formulas on an LRFD basis. *Struct J*. 1996;93(1):128–37.
  64. Jonak J. Kotwa podcinająco-odspajająca Nr zgłoszenia patentowego A 429560. *Biuletyn Urzędu Patentowego: Wynalazki i Wzory użytkowe*, 2019, 25; 41.
  65. Szkudlarek Z, Podgórski J, Jonak J. Numerical simulation of rock separation process by cutting prissing head. *Maint Reliab*. 2004;54–7.